EUMETSAT

OSI SAF

OCEAN AND SEA ICE

Algorithm theoretical basis document for the OSI SAF 50GHz sea ice emissivity model

OSI-404-a

Version: 2.2

Date: 01/05/2018

Rasmus T. Tonboe

Document Change record

Document version	Software version	Date	Author	Change description
V1.0		Dec. 2010	R. Tonboe and H. Schyberg	For review
V1.1		Oct. 2011	R. Tonboe and H. Schyberg	Response to review comments
V2.0		Feb. 2017	R. Tonboe	For PCR review
V2.1		April 2017	R. Tonboe	Response to review comments
V2.2		April 2018	R. Tonboe	Response to reviewer comments

Table of contents

1.Introduction....3
1.1.Scope of this document....4
1.1.1.Disclaimer....4
1.2.Reference documents....4
1.3.Glossary....5
1.4.Emissivity models....5
2.The semi-empirical emissivity model....7
3.Special Sensor Microwave Imager/Sounder (SSMIS)....8
4.GCOM-W1 AMSR2....9
5.The cross track scanning microwave sounding unit (AMSU)....9
6.The microwave emission model....10
7.Sea ice thermodynamic and mass model....12
8.The interface between the thermodynamic and the emission model....13
9.Algorithm Description: the emissivity model....14
9.1.Functionality of the model....19
10.Update of the algorithm coefficients using the validation product as a reference....23
11.The effective temperature....24
12.Processing....26
13.Validation/comparison plan....27
14.Acknowledgements....27
15.References....29

1. Introduction

The sea ice surface brightness temperature, Tb, is the product of the effective temperature, Teff, and the emissivity, e, i.e. Tb=Teff*e under the assumption of constant temperature and homogeneous conditions. These conditions are rarely found in reality but the e and Teff anyway make sense as counterparts in describing the self-emission from the surface (Tb), and the emissivity, the reflectivity of atmospheric down welling radiation (r=1-e). Atmospheric absorption, emission and scattering are not included. The effective temperature is the integrated emitting layer thermometric temperature. This report describes an algorithm for deriving the 50GHz sea ice emissivity its level of specularity and the effective temperature.

Atmospheric temperature sounding applications (such as NWP assimilation) near 50GHz over sea ice is the motivation for this study. English (1999, 2008) shows that nearly as much information about atmospheric humidity can be retrieved from e.g. sea ice covered regions as over the open ocean if the emissivity is less than 0.95, the emissivity uncertainty is less than 2 %, and the skin temperature uncertainty is less than 2 K. These accuracies have been difficult to achieve in practise over sea ice. However, test runs with the regional NWP model HIRLAM where satellite microwave radiometer data from sea ice covered regions were assimilated indicated that atmospheric temperature sounding over sea ice is in fact feasible. The test runs were using a simple sea ice surface emissivity model and it showed that the assimilation of AMSU near 50 GHz temperature sounding data improved model skill on common variables such as surface temperature, wind and air pressure (Heygster et al., 2009). The sea ice effective temperature is also important for the atmospheric sounding applications (English, 2008). The effective temperature is described in Tonboe et al. (2011) and an estimate based on AMSR 6 and 10 GHz Tb data is described in this report.

Transmission of microwave radiation through the atmosphere in the range from 6 to 183 GHz is affected primarily by three processes: 1) oxygen absorption particularly from 50 to70 GHz and near 118 GHz, 2) water vapour absorption especially near 22 GHz and 183 GHz, and 3) scattering from water and ice particles in particular at higher frequencies and dependent on the incidence angle i.e. path length through the atmosphere. Near the 183 GHz water and the 50-70 GHz and 118 GHz oxygen absorption lines the atmosphere is virtually opaque and the satellite channels measuring at or near these frequencies are called sounding channels. However, there is a potential contribution from the surface at the lower temperature sounding frequencies between 50.3 and 54.4 GHz where microwave penetration is into the troposphere. These frequencies correspond for example to channels 3-6 on the Advanced Microwave Sounding Unit (AMSU) instrument and the channels between 50.3 and 54.4GHz on the Special Sensor Microwave Imager/ Sounder (SSMIS). The polar atmosphere is generally transparent for microwave radiation in between the sounding channels called the atmospheric windows near 18, 36, 90, and 150 GHz. For typical polar atmospheric states the down-welling emission at the surface is about 5-15 K at 18 GHz, 20-40 K at 36 GHz, 30-100 K at 89 GHz. The sea ice surface emission is typically 150-260 K for comparison. The sea ice emissivity, at a certain polarisation, frequency and angle with respect to the surface, is a function of subsurface extinction and reflections between snow layers with different permittivity. The microwave penetration depth in snow and ice is in the order of centimetres to decimetres due to significant extinction in the snow and absorption in saline ice. Physical models relate the emissivity with the snow and ice properties such as density, temperature, snow crystal and brine inclusion size to microwave attenuation, scattering and reflectivity.

We are simulating 50 GHz sea ice emissivities using SSMIS and AMSR-2 microwave radiometer data as input and assuming that the angular variation can be described by the Fresnel reflection equations scaled in magnitude and polarisation whith empirically derived coefficients, We validate our results using emissivities derived directly from the 50 GHz and 52 GHz channels on the SSMIS microwave radiometer and using numerical weather prediction data and a radiative transfer model.

The brightness temperatures measured at each frequency have different spatial resolution on the Earth surface. In particular there are large differences between the 6 GHz resolution on AMSR (FOV 74x43 km = 3064 km^2) used for ice temperature estimation and the 18 to 36 GHz (FOV 27x16 km = 864 km^2 and 14x8 km = 486 km^2) brightness temperatures used for deriving the emissivity.

The sea ice emissivity uncertainties are computed as a 3 by 3 pixel STD of the difference between the product and validation product emissivities. This is a local uncertainty on every pixel. The hemispheric product and validation product STD is including potential biases between the two products.

1.1. Scope of this document

This Algorithm Theoretical Basis Document describes the computational steps for a sea ice emissivity model which is implemented as part of the EUMETSAT OSI SAF programme. The document introduces and justifies the scientific assumptions and choices which are made. It does not deal with all aspects of the processing. Important issues for example resolution matching, atmospheric correction of brightness temperatures, output format and quality control are not part of this document. These things are described in the reference documents: The OSI-PRD-PRO-205 in the OSI SAF Product Requirement Document referred to as [RD.1]. The validation results are presented in the validation report referred to as [RD.2]. The data are presented in the product users manual referred to as [RD.3].

A new validation methodology was introduced in 2016 for daily and continuous validation of the emissivity product. The validation has resulted in an update of the emissivity algorithm coefficients. The description of this update is the primary addition to version 2.0 of this report (from v1.1).

General information on the EUMETSAT OSI SAF and the reference documents are available from the OSI-SAF official web site: www.osi-saf.org.

1.1.1. Disclaimer

1.2. Reference documents

Reference documents

[RD.1] OSI SAF

CDOP 3 Product Requirement Document (PRD)

SAF/OSI/CDOP3/MF/MGT/PL/2-001, Version 1.1, 20/11/2017

[RD.2] OSI SAF

Validation of the 50 GHz sea ice emissivity product

SAF/OSI/CDOP3/DMI/TEC/RP/190, Version 1.6, May 2018

[RD.3] OSI SAF

Product Users Manual for the OSI SAF 50GHz sea ice emissivity product.

SAF/OSI/CDOP3/DMI/TEC/MA/191, Version 1.6, May 2018

[RD.4] OSI SAF

Service Specification (SeSp)

SAF/OSI/CDOP3/MF/MGT/PL/003, Version 1.3, 14/12/2017

Reference to a reference Document within the body of this document is indicated as reference in the list above, e.g. [RD.1].

1.3. Glossary

AMSR - Advanced Microwave Scanning Radiometer

AMSU - Advanced Microwave Sounding Unit

ATBD - Algorithm Theoretical Basis Document (This document)

CDOP – Continuous Development and Operations Phase

DMI – Danish Meteorological Institute

EUMETSAT - European Organisation for the Exploitation of Meteorological Satellites

FOV - Field of View

HIRLAM - High Resolution Local Area Model

Metop – EUMETSAT OPerational METeorological polar orbiting satellite

NWP - Numerical Weather Prediction

OSI SAF – Ocean and Sea Ice Satellite Application Facilities

SSM/I - Special Sensor Microwave/Imager

SSMIS - Special Sensor Microwave Imager/Sounder

1.4. Emissivity models

The sea ice surface emissivity at 50GHz is high compared to the open ocean for most ice types and penetration through the atmosphere at humidity sounding channels can be significant because the Arctic atmosphere is often very dry. Getting a good estimate of sea ice emissivity is more complicated than over the open ocean. Compared to the open ocean microwave emissivity the complications for sea ice are that there are large vertical and lateral surface heterogeneity within the foot-print including significant microwave penetration into the snow and ice and across the temperature gradient beneath the surface meaning that the surface temperature is not synonymous with the effective temperature. NWP models don't typically contain as state variables the parameters necessary to drive microwave emission

models. The sea ice is dynamic: it drifts, deforms, melts or forms with significant changes from day to day which means that emissivity climatology is not as valid as it is over land without snow cover.

For smooth soil surfaces the surface reflectivity is specular, otherwise for rough surfaces the specular model can be adjusted using a single-parameter (roughness) model (Ulaby et al. 1982, p. 889) i.e.

$$r(\theta, p) = r_{sp}(\theta, p) e^{-h' \cos^2 \theta} \quad (1),$$

where r is the reflectivity at incidence angle θ and v or h polarisation p. The subscript sp is for specular and h' is a roughness parameter.

Several models link the physical snow and ice properties with the microwave emission (e.g Tonboe et al. 2006; Weng et al. 2001). The community microwave emission model for land surfaces uses a combination of rough and specular surface scattering where the surface roughness state is derived from auxiliary parameters e.g. land use maps (Drusch et al., 2009).

Mätzler and Rosenkranz (2007) describe the bistatic scattering near Dome C in Antarctica and compare with AMSU A measurements at 31 and 50GHz. They find that the snow surface scattering is diffuse and that the Lambertian model rather than the specular model makes a good fit to measurements. This means that the angular response of the AMSU near 50GHz emissivity is small. They also find that there is a crossover between the specular and the Lambertian models near 50deg of incidence so that coincidently both models would predict the same outcome for conically scanning radiometers operating at incidence angles near 50deg (e.g. SSM/I, SSMIS, AMSR). The Lambertian model implies that there is no polarisation difference at oblique incidence angles. However, as they mention, there is a significant polarisation difference at e.g. 19, 37 and at 89GHz and this is also the case at 50 GHz. Therefore, the surface cannot be truly Lambertian and Mätzler (2005) simulates the emissivity of snow surfaces as a mix between Lambertian and specular scattering. The surface emissivity model input parameters are not prognostic variables in NWP models and they are difficult to simulate. These input parameters in for example MEMLS include, for instance, the grain size or correlation length vertical profiles within the snow-pack which are difficult to measure in the field and are a stretch target for detailed process models at present. In addition, most atmospheric models treat the surface as purely specular with the exception of that used by Guedj et al. (2010).

2. The semi-empirical emissivity model

Therefore, the microwave emissivity near 50GHz is characterised here using a model where the emissivity at 50º is a function of the spectral gradient and the polarisation ratio measured at the neighbouring atmospheric window frequencies at 18 and 36 GHz. The PR and GR can be measured with SSM/I, AMSR and SSMIS sensors currently in orbit. Output from a combined 1D thermodynamic and a microwave emission model is used for generating the relationships between the emission at 50 GHz at 50º of incidence and the 18 GHz and 36 GHz simulated brightness temperatures. The approaches of both the community model (Drusch et al., 2009) and Mätzler's model (Mätzler, 2005) find solutions between two extreme cases. Similarly this model can attain solutions in between: 1) perfectly diffuse emission where there is no angular dependence and no polarisation difference similar to the model used in Heygster et al. (2009), and 2) the specular reflection with the angular dependence and the polarisation determined by the Fresnel reflection coefficients and a surface permittivity of 3.5 which is typical for sea ice. The model is expected to be valid for incidence angles between 0º and 60º and cases in between the two extremes.

Brightness temperatures are measured at window frequencies where the sensitivity to the atmosphere is minimized e.g. at 18 and 36 GHz. The spectral gradient (GR1836V) is given by the following equation:

$$GR1836V = \frac{T_{v36} - T_{v18}}{T_{v36} + T_{v18}} \quad (2).$$

The normalisation reduces the GR sensitivity to effective temperature, and ice concentration algorithms use it to correct for first- and multiyear ice types with different volume scattering magnitudes (Comiso et al., 1997). Though the sensitivity to temperature (Teff) is reduced in GR there is still a reminiscent due to different microwave penetration at 18 and 36 GHz across the temperature gradient in snow and ice.

The polarisation ratio at 36 GHz, PR36, is given by the difference over the sum of the Tv36 and Th36 brightness temperatures at 36GHz, i.e

$$PR36 = \frac{T_{v36} - T_{h36}}{T_{v36} + T_{h36}} \quad (3).$$

Also for the polarisation ratio the temperature dependence is minimized by the normalisation.

3. Special Sensor Microwave Imager/Sounder (SSMIS)

The SSMIS is a polar orbiting satellite with a conically scanning microwave radiometer with constant incidence angle around 50º and a swath width of about 1700km. It has window channels near 19, 37, 91, and 150GHz and sounding channels near 22, 50, 60, and 183 GHz. The SSMIS temperature sounding channels 1-4 near 50 GHz vertical polarisation penetrate into the lower troposphere and partially to the surface (Kunkee et al., 2008).

Table 1 shows the SSMIS channels.

Central frequency (HZ)	Bandwidth (MHz)	Polarisation	Accuracy (NEΔT)	IFOV	Pixel
19.35	400	V, H	0.7K	45X68 km	25X12.5 km
22.235	400	V	0.7K	40X60 km	25X12.5 km
37.0	1500	V, H	0.5K	24X36 km	25X12.5 km
50.3	400	H	0.4K	18X27 km	37.5X12.5 km
52.8	400	H	0.4K	18X27 km	37.5X12.5 km
53.596	400	H	0.4K	18X27 km	37.5X12.5 km
54.4	400	H	0.4K	18X27 km	37.5X12.5 km
55.5	400	H	0.4K	18X27 km	37.5X12.5 km
57.29	350	-	0.5K	18X27 km	37.5X12.5 km
59.4	250	-	0.6K	18X27 km	37.5X12.5 km
60.792668± 0.357892± 0.050	120	V+H	0.7K	18X27 km	37.5X12.5 km
60.792668± 0.357892 ± 0.016	32	V+H	0.6K	18X27 km	75.0X12.5 km
60.792668± 0.357892 ± 0.006	12	V+H	1.0K	18X27 km	75.0X12.5 km
60.792668± 0.357892 ± 0.002	6	V+H	1.8K	18X27 km	75.0X12.5 km
60.792668± 0.357892	3	V+H	2.4K	18X27 km	75.0X12.5 km
63.283248± 0.285271	3	V+H	2.4K	18X27 km	75.0X12.5 km
91.655	3000	V, H	0.9K	10X15 km	12.5X12.5 km
150	1500	H	0.9K	...X... km	37.5X12.5 km
183.31 ± 6.6	1500	H	1.2K	...X... km	37.5X12.5 km
183.31 ± 3.0	1000	H	1.0K	...X... km	37.5X12.5 km
183.31 ± 1.0	500	H	1.2K	...X... km	37.5X12.5 km

Table 1. The channels on SSMIS (http://www.wmo.int/pages/prog/sat/Instruments_and_missions/SSMIS.html).

4. GCOM-W1 AMSR2

The Advanced Microwave Scanning Radiometer 2 (AMSR2) onboard the GCOM-W1 satellite is a conically scanning microwave radiometer measuring from a polar orbit at about 700 km above the Earth's surface and obtains data over a 1450 km swath at an incidence angle of 55deg.It measures at both linear vertical and horizontal polarisation at 6.9, 7.3, 10.7, 18.7, 23.8, 36.5, 89 GHz.

5. The cross track scanning microwave sounding unit (AMSU)

The AMSU instrument is a whisk broom polar orbiting microwave radiometer with variable incidence angle, foot-print size and the linear polarisations are mixed. Similar instruments have been in orbit since the 1970s. AMSU has scan angles between nadir and about +/-49º and a swath with of about 2000 km. Provided that the 3rd and 4th Stokes parameters are near 0 over sea ice the h and v polarisations are mixed as a function of scan angle, θ, on AMSU (Mathews et al., 2009):

$$\varepsilon(\theta) = \varepsilon_v(\theta)\cos^2(\theta_s) + \varepsilon_h(\theta)\sin^2(\theta_s) \quad (4),$$

where

$$\theta_s = \arcsin\left(\frac{R_e}{R_e + H}\sin(\theta)\right) \quad (5).$$

R_e is the Earths radius (6371km) and H is the height of the satellite above the surface (about 800km). The 3rd and 4th Stokes parameters are most often near zero during the cold season (Narvekar et al., 2011). Figure 1 shows the channels on AMSU A and the atmospheric absorption spectra.

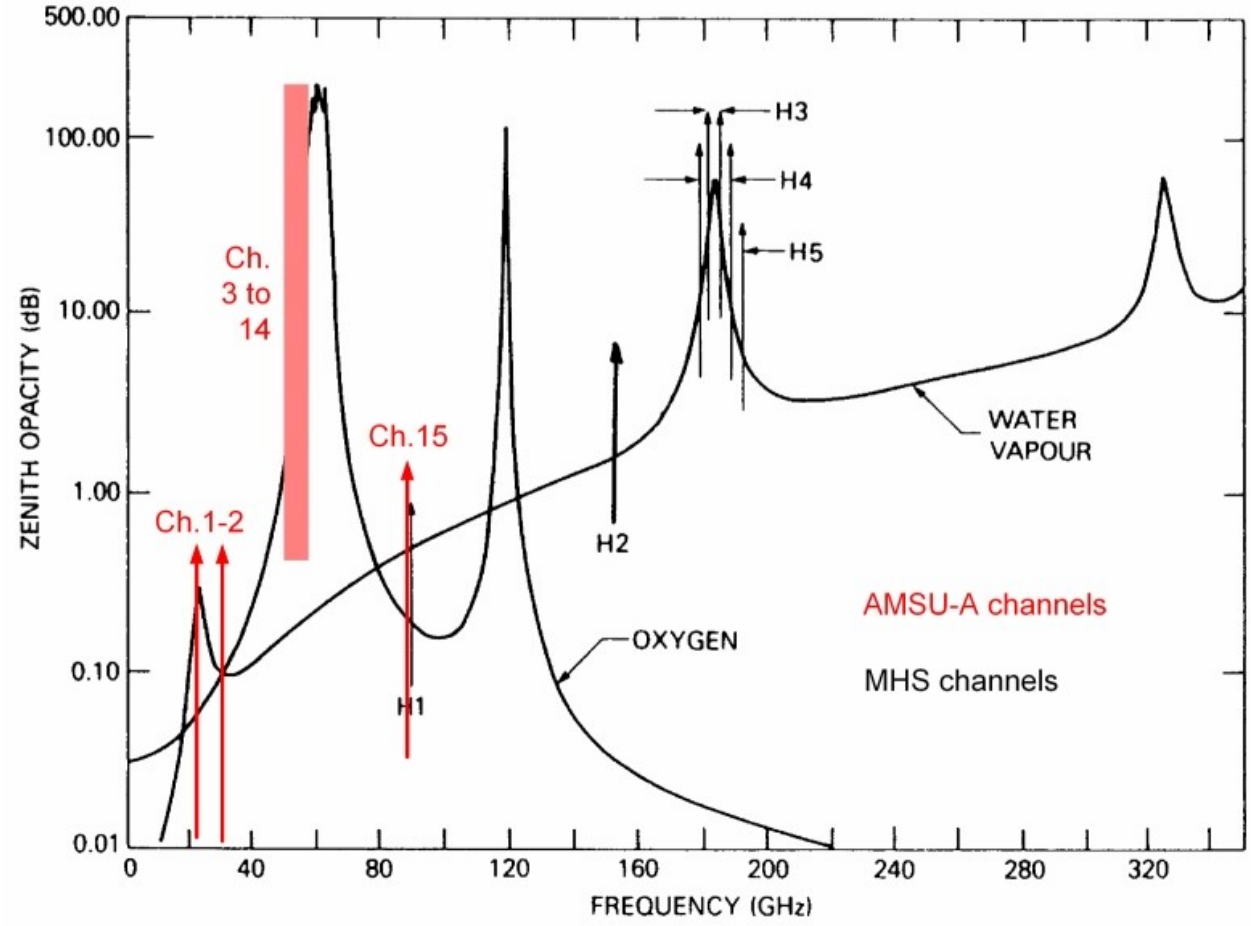

Figure 1 : The atmospheric absorption spectra and the channels on AMSU-A (figure from EUMETSAT homepage).

6. The microwave emission model

Simulated data from a combined thermodynamic and emission model is used to derive the coefficients for the OSI SAF 50GHz emissivity model. The sea ice emission model relate physical snow and ice properties such as density, temperature, snow crystal and brine inclusion size from the thermodynamic model to microwave attenuation, scattering and reflectivity. The emission model used here is a sea ice version of MEMLS (Wiesmann and Mätzler, 1999) described in Mätzler et al. (2006).

The theoretical improved Born approximation was used here, which validate for a wider range of frequencies and scatterer sizes than the empirical formulations (Mätzler and Wiesmann, 1999). Using the improved Born approximation the shape of the scatters is important for the scattering magnitude (Mätzler, 1998). We assume spherical scatters in snow when the correlation length pec, a measure of grain size, is less than 0.2 mm and the scatters are formed as cups when greater than 0.2 mm to resemble depth hoar crystals.

The sea ice version of MEMLS includes models for the sea ice dielectric properties while using the same principles for radiative transfer as the snow model. Again the scattering within sea ice layers be-

neath the snow is estimated using the improved Born approximation. The scattering in first-year ice and multiyear ice is assumed from small brine pockets and air bubbles within the ice respectively.

All simulations are at 50 degrees incidence angle similar to SSMIS and other conically scanning radiometers.

7. Sea ice thermodynamic and mass model

In order to produce input to the emissivity model a one dimensional snow/ice thermodynamic model has been developed. Its purpose is not necessarily to reproduce a particular situation in time and space rather to provide realistic microphysical input to the emissivity model. Earlier thermodynamic models such as Maykut and Untersteiner (1971) or even simple degree day models (see e.g. Maykut, 1986) are useful for simulating ice thickness. However, for microwave emission modelling applications additional parameters such as temperature, density, snow grain size and ice salinity at very high vertical resolution are needed. Because the thermal conductivity is a function of temperature the model uses an iterative procedure between each time step of six hours. The thermodynamic model is fed with ECMWF ERA40 data input at these six hours intervals. In return the thermodynamic model produces detailed snow and ice profiles which are input to the emission model at each time step. This gives a picture of significant emission processes in sea ice even though the one dimensional thermodynamic model is not capturing the spatial variability of the sea ice cover caused for example by ice convergence resulting in deformation, ice divergence resulting in new-ice formation, and wind redistribution of the snow cover affecting snow depth, density and grain size. The thermodynamic model has the following prognostic parameters for each layer: thermometric temperature, density, thickness, snow grain size and type, ice salinity and snow liquid water content. Snow layering is very important for the microwave signatures therefore it treats snow layers related to individual snow precipitation events. This means that if a snow precipitation event deposits a new snow layer then that is a new layer in the model and this layer is followed to the end of the simulation. The initial depth of the snow layer is a function of the mass of precipitation, and density, initially a function of temperature and wind speed at time of deposition. Snow layers compact due to loading and metamorphosis. For sea ice it has a growth rate dependent salinity profile. New ice layers are 5 cm when they are closed in the model. The sea ice salinity for each new added layer (bottom growth) is a function of growth rate, u, and water salinity, S_w (Nakawo and Sinha, 1981), i.e.

$$S = 0.12 S_w / \{0.12 + 0.88 \exp(-4.2 \times 10^4 u)\} \quad (6),$$

The water salinity is 32 psu and the growth rate is in cm/day.

The thermodynamical model is used for simulating detailed profiles which are used as input to the emission model. Six different positions all within the Arctic Ocean were selected for having different meteorological conditions, snow pack development and ice growth. The set-up is illustrated and explained in Tonboe (2010). Climatology indicates that there is snow on multiyear ice at the end of summer melt in September (Warren et al., 1999). Therefore, the multiyear ice simulations are initiated on 1 September with an isothermal 2.5 m ice floe with 5 cm old snow layer on top. The multiyear ice gradually grows at the six positions from 2.5 m to between 3.0 m and 3.4 m in spring and snow depths during winter range between 0.2 m and 0.5 m. The melt processes during the summer season are complicated and not sufficiently described by the thermodynamic model. Summer melt is therefore not included in this study. The thermodynamic model is further described in Tonboe (2005, 2010).

8. The interface between the thermodynamic and the emission model

Snow grain size affects both shortwave extinction in the thermodynamic model and microwave scattering in the emission model. The emission model is using p_{ec} as a measure of grain size and the optical grain diameter D_0 forms the interface between the two models. There are no snow metamorphosis relationships in terms of p_{ec} so the conversion between terms is needed. It is assumed that grain size and p_{ec} evolve similarly during metamorphosis and our grain size growth model is not dependent on initial grain size. Therefore the conversion factor F is not critical. We use F=0.4 and the correlation length, $p_{ec,}$ of new snow deposits is set to 0.07 mm which is typical for new snow (Wiesmann et al., 1998). Grain growth is not assigned to the top snow layer. Other microphysical parameters in the profile such as physical temperature, density, salinity are used directly in the emission model.

According to Marbouty's (1980) temperature gradient metamorphism model for dry snow, used in the thermodynamic model, the mean grain size diameter (D_m) growth is a function of temperature gradient, temperature and density. Baunach et al. (2001) and Jordan et al. (1999) indicate that the growth rate is also a function of the initial grain size. However, as a first approximation Marbouty's model gives a good fit to observations and for conversion to other structural parameters in the two models it is an advantage that growth rate is independent of initial size. For example, the shortwave extinction in the snow is a function of the snow density and the optical grain diameter (D_o) (Brun et al., 1992). Since growth rate is independent of initial size D_m can be set equal to the diameter of equally sized spheres (D). D is related to D_o by (Mätzler, 2002), i.e.

$$D = D_o(1-v) \quad (7),$$

where

$$v = \rho_{snow} / \rho_{ice} \quad (8).$$

The ρ_{snow} is the snow density and ρ_{ice} is the ice density. The emission model is using the exponential correlation length (p_{ec}) a structural parameter of scatter size and distribution (Mätzler, 1998). Mätzler (2002) analyses different relationships between the snow structure, grain size and the correlation length. D_o is related to p_{ec} for rounded grains, i.e.

$$p_{ec} = FD_o \quad (9),$$

where F is 0.16 for snow grain sizes modelled with SNTHERM, 0.3-0.4 for Crocus grain sizes and types, and 0.16 for fine grained snow and 0.25 for medium grained snow using a one dimensional scattering model. It is further suggested to include the snow density, i.e.

$$p_{ec} = 0.5D_o(1-v) \quad (10).$$

For realistic snow densities between 150-400 kg/m^3 the factor 0.5(1-v) is 0.28-0.41, i.e. the factor F in Eq. 9. These relationships are not strictly valid for new-snow and depth hoar where the grains are not rounded (Mätzler, 2002).

9. Algorithm Description: the emissivity model

The sea ice emissivity at 50 GHz is related to the GR1836. Simulated data for both the vertical and horizontal polarisation at an incidence angle of 50º are shown in figure 2 and 3. The combination of GR1836 at vertical polarisation, we denote it GR1836V, and ev is the least noisy and has fewest outliers and it is therefore used in the algorithm. The figures 2 and 3 are shown to illustrate the GR and emissivity relationships.

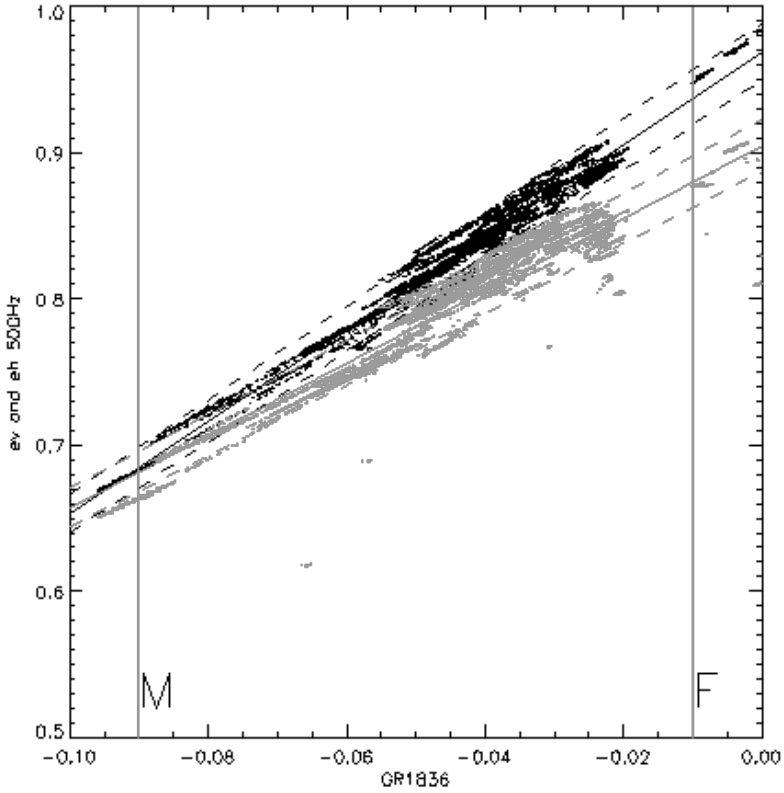

Figure 2 : The simulated multi-year ice GR1836V vs. the e_{50v} (black) and e_{50h} (grey). The best fit line to the e_{50v} is: e_{50v}=3.16GR1836V+0.97 and for e_{50h}: e_{50h}=2.48GR1836V+0.90. The dashed lines show the +/-2%. The vertical grey lines indicate the tie-points for first- (F) and multiyear (M) ice respectively.

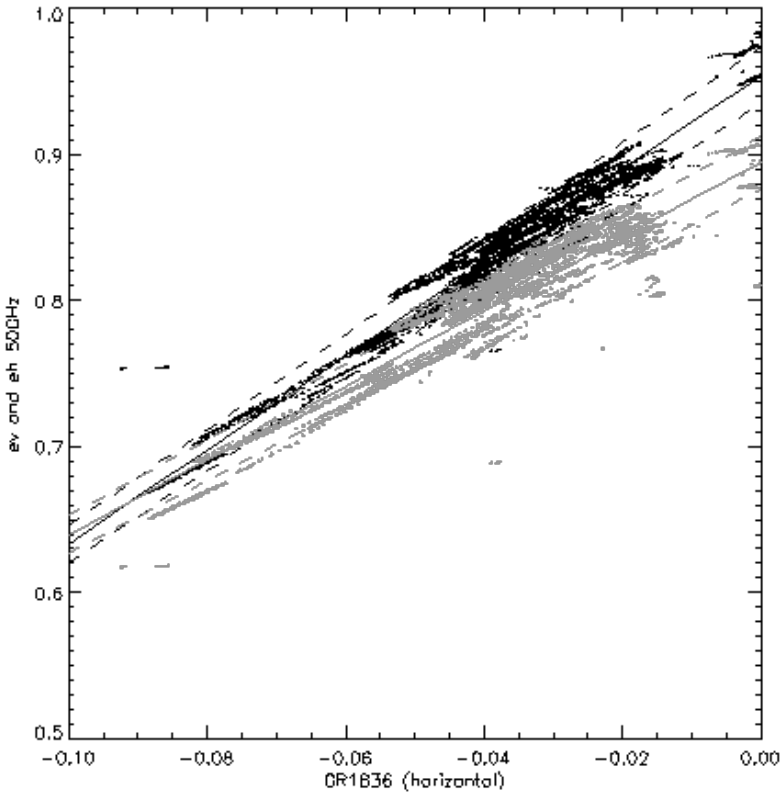

Figure 3: The simulated multi-year ice horizontal GR1836H vs. the e_{50v} (black) and e_{50h} (grey). The best fit line to the e_{50v} is: e_{50v}=3.21GR1836H+0.95 and for e_{50h}: e_{50h}=2.54GR1836H+0.89. The dashed lines show the +/-2%. The figure is the same as figure 1 except the gradient is at horizontal polarisation.

The model and the simulations are described in Tonboe (2010). Figure 3 is as Figure 2 except that it is showing the emissivity as a function of the gradient at horizontal polarisation. Lines have been fitted to the data clusters representing simple models for the emissivity, i.e.

$$e50v(GR1836\mathrm{V}) = 3.16GR1836\mathrm{V} + 0.97 \quad (11),$$

and

$$e50h(GR1836) = 2.48GR1836\mathrm{V} + 0.90 \quad (12).$$

It is noted that both the emissivity and the polarisation difference are decreasing as a function of larger negative GR1836V. Most of the simulated data points are within +/-2% of the fitted lines and the model - data RMS for vertical polarisation is 0.008 (for the southern hemisphere the RMS is 0.01) and the RMS is 0.019 for horizontal polarisation. The crossover of the fitted lines in Figure 2 is not physical and the v - h polarisation difference is always positive as illustrated in Figure 4.

The GR1836V Arctic tie-points for first and multiyear ice are shown in Figure 2. The tie-points from Comiso et al. (1997) represent typical values for the two ice types respectively.

The GR1836V vs. the e50 polarisation difference is illustrated in Figure 4. This relationship is noisy and therefore the GR1836V cannot be used for deriving the polarisation difference.

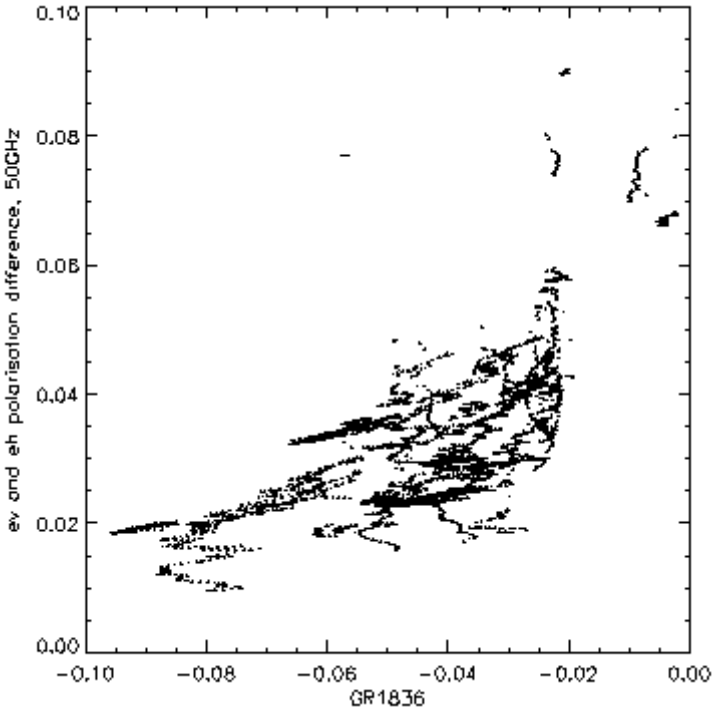

Figure 4: The emissivity polarisation difference at 50GHz vs. the GR1836V.

Instead we use the relationship between PR36 and PR50 shown in figure 5 where the polarisation ratio at 36 GHz is a proxy for the polarisation difference at 50 GHz. The model - data RMS for the 36GHZ polarisation ratio and the 50GHz polarisation ratio is 0.0014. The same processes determine the polarisation difference at 36 GHz and at 50 GHz.

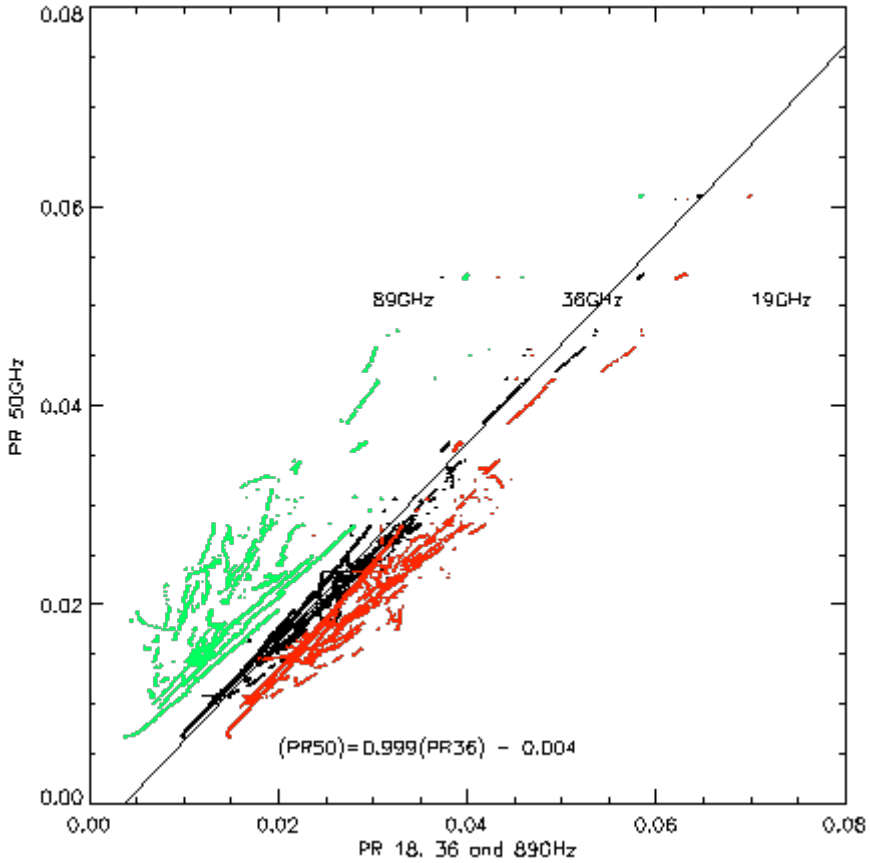

Figure 5: The simulated sea ice PR18 in red, PR36 in black, and PR89 in green vs. the PR50.

There is a near 1:1 relationship between the polarisation ratio at 36 GHz and at 50 GHz.

Using the linear relationships in figure 2 and 5 based on the simulated data it is now possible to estimate the 50 GHz emissivity at 50º incidence at vertical and horizontal polarisation in terms of GR1836V and PR36. The PR is decreasing from 19 GHz to 36 GHz to 50 GHz and to 89 GHz.

Here we propose a simple model for extrapolating the GR1836V emissivity proxy and the PR36 polarisation proxy for SSMIS to the range of incidence angles (θ) and h and v polarisation on AMSU using the reflection coefficients for sea ice. The specular reflection coefficients for vertical, r_v, and horizontal, r_h, polarisation is given in terms of the sea ice permittivity ε (ε=3.5) and θ the angle of incidence, i.e.

$$r_v(\theta) = \left| \frac{\varepsilon \cos\theta - \sqrt{\varepsilon - \sin^2\theta}}{\varepsilon \cos\theta + \sqrt{\varepsilon - \sin^2\theta}} \right|^2 \quad (13).$$

$$r_h(\theta) = \left| \frac{\cos\theta - \sqrt{\varepsilon - \sin^2\theta}}{\cos\theta + \sqrt{\varepsilon - \sin^2\theta}} \right|^2 \quad (14).$$

If the sea ice absorption is considered as well i.e. the permittivity is 3.5+0.5j instead of 3.5, which is a high loss factor typical for warm and saline sea ice, then the difference in emissivity between permit-

tivities 3.5 and 3.5+0.5j is less than 0.003 between 0 and 60 degrees. For 3.5 and 3.5+0.1j which is realistic for cold ice it is less than 0.0002. These differences are small compared other uncertainties in particular during the cold season.

The 50 GHz emissivity is in terms of the two parameters S and R:

$$e_{50h}(\theta) = S\{1 - Rr_h(\theta)\} \quad (15),$$

and

$$e_{50v}(\theta) = S\{1 - Rr_v(\theta)\} \quad (16).$$

The RMS between the emissivity from the radiative transfer model (in Tonboe, 2011) and the model in eq. 15 and 16 at 50 degrees incidence angle is 0.0071 for horizontal polarisation and 0.0093 for vertical polarisation. In the Ulaby et al. (1982) model shown in eq. 1 R is a surface roughness parameter. For the totally diffuse surface S is equivalent to the emissivity and S is a scaling parameter of the emissivity. Here because of the relationship between the PR36 and PR50 R is given as a function of PR36 shown in Figure 6. A 3rd degree polynomial is fitted to the simulated data (Tonboe, 2010) using least squares for the northern and southern hemisphere, i.e.

North $R(PR36) = 0.000215 + 10.238PR36 - 11.492PR36^2 + 9.286PR36^3$

South $R(PR36) = 0.000471 + 10.22PR36 - 11.02PR36^2 + 5.93PR36^3$ (17).

and S as a function of GR1836V shown in Figure 7 using least squares:

North $S(GR1836V) = 3.185GR1836V + 0.978$

South $S(GR1836V) = 3.13GR1836V + 0.96$ (18).

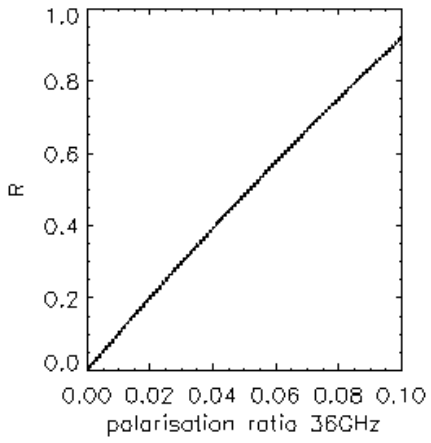

Figure 6: The R as a function of PR36. The line shows the fit to the simulated data.

For R = 0 the scattering at the surface is totally diffuse and for R = 1 the scattering is specular. R = 1 for PR36 = 0.11 at sea ice permittivity of 3.5.

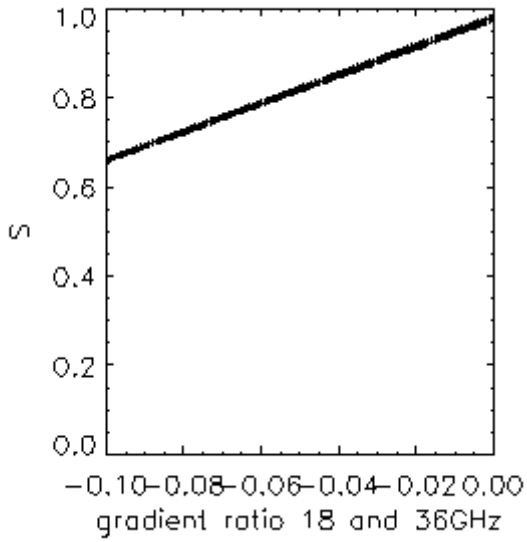

Figure 7: The S as a function of GR1836V. The line shows the fit to the simulated data.

The scattering of points around the line is because S is also a weak function of PR36, however this is neglected here.

9.1. Functionality of the model

The emissivity as a function of incidence angle is shown for three cases: 1) the totally diffuse case where the PR36 equals 0, i.e. there is no polarisation difference, in Figure 8, and 2) the specular case where PR36 equals 0.11 at sea ice permittivity of 3.5 and the emissivity is detirnined by the Fresnel reflection coeffiecents in Figure 9, and 3) the intermediate a combination of diffuse and specular scattering case where GR1836V equals -0.08 and PR36 equals 0.02 in Figure 10.

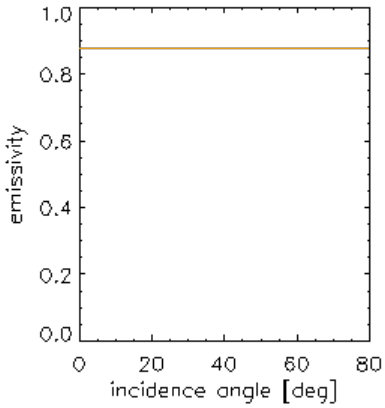

Figure 8: The totally diffuse case where PR36 = 0 and GR1836V = -0.03, The yellow line shows the e_{AMSU}, e_v and e_h.

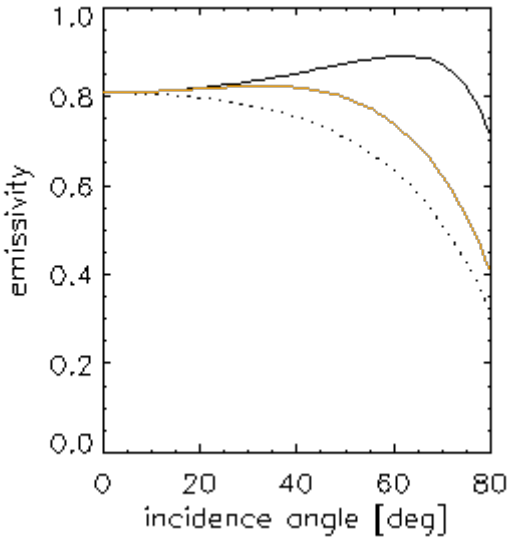

Figure 9: The specular case (R=1) where PR36 = 0.11 and GR1836V = -0.03. The yellow line shows the e_{AMSU}, the black full line the e_v and the dotted line the e_h.

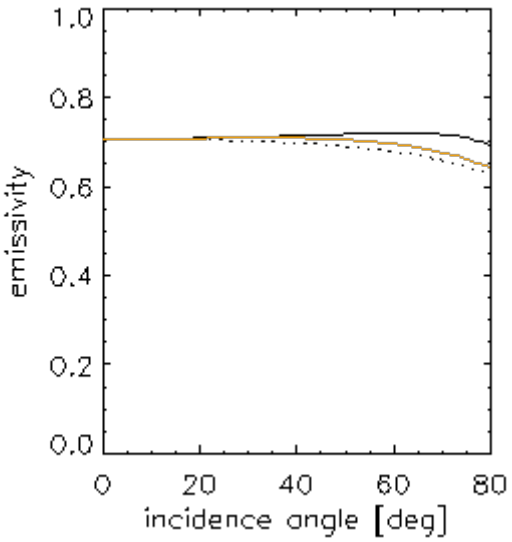

Figure 10: The intermediate case where PR36 = 0.02 and GR1836V=-0.08 (typical for multiyear ice). The yellow line shows the e_{MSU}, the black full line the e_v and the dotted line the e_h.

The e50v at 50º of incidence is shown in figure 11.

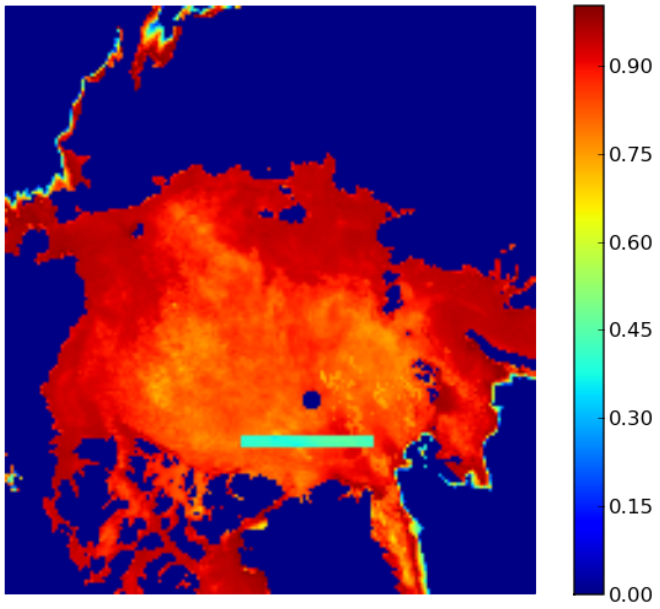

Figure 11: The 50GHz emissivity at vertical polarisation and at 50º incidence angle 1. Jan. 2003. The cyan rectangle is the area selected for data to figures 12 and 13.

The brightness temperature at 6, 18 and 36GHz vertically polarised AMSR channels is shown in Figure 12 for a small area north of Greenland shown with cyan in Figure 11 predominantly covered by multiyear ice.

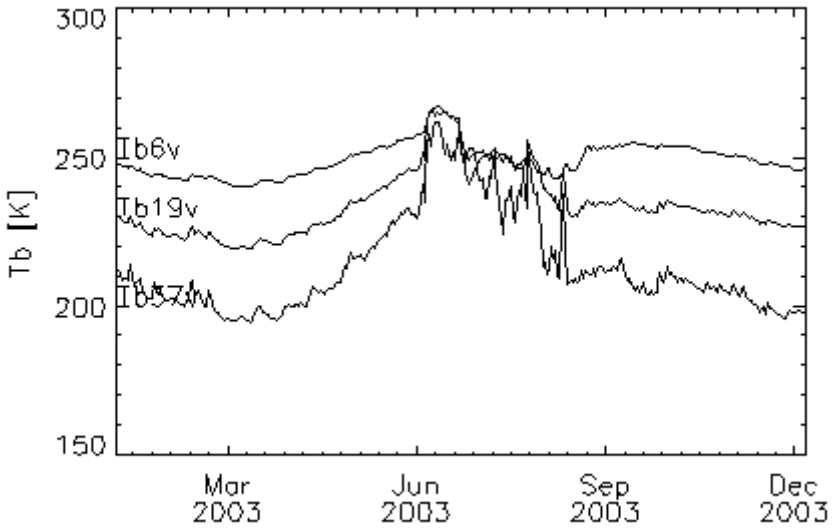

Figure 12: Brightness temperatures, Tb, north of Greenland

Figure 13 shows the model coefficients R and S derived from AMSR data in the small area north of Greenland.

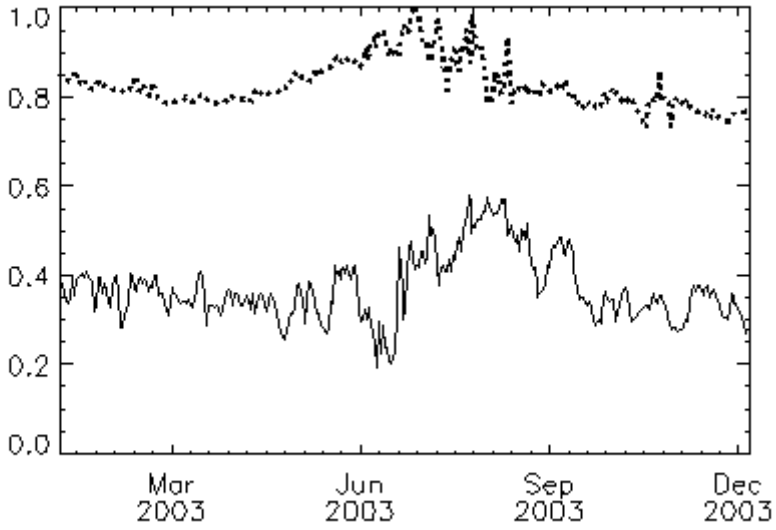

Figure 13: S (dashed) and R (solid) for multiyear ice north of Greenland

The algorithm is valid both summer and winter. It is clear that the coefficients are affected by summer melt (Fig. 13) and the uncertainties become larger during summer. This is described further in the validation report. This is due to a more uncertain estimation of the regions with near 100% sea ice and possibly atmospheric emission and scattering.

10. Update of the algorithm coefficients using the validation product as a reference

A bias has been observed in the first version of the product compared to the validation product. In order to correct this bias we have tuned the model coefficients of the operational product to the validation product as described in this section.

For the totally diffuse situation where there is no polarisation difference where R equals 0 (actually in this model it is about 2e-04 which is close enough to zero) the algorithm coefficient S is equivalent with the ev50. Even in other more specular situations (R>0) S scales with ev50 linearly (see figure 7). The validation product provides ev50 at an incidence angle of 53deg. for comparison. The comparison between the product ev50 and the validation ev50 shows that there is a bias between the product and the validation and the bias is different for high and low emissivities in the current setup (Feb. 2017). We have selected the year 2016 for comparing the product (ev50_prod) and the validation (ev50_val) emissivities and computed the slope and offset for lines fitting the cluster of points every day of the year and for both hemispheres separately. The yearly average for north and south are:

North: ev50_val = 0.87ev50_prod + 0.014 (19)

South: ev50_val = 0.84ev50_prod + 0.032

For the case where R=0 (diffuse) we replace ev50_val with S and enter equations 19 in equation 18 to get an updated set of equations for S in equations 20:

North: S = 2.764GR1836V + 0.8624 (20)

South: S = 2.6438GR1836V + 0.8426

Test runs show that the updated equations for S (eq. 20) removes the hemispheric bias between the product and the validation emissivity.

11. The effective temperature

The snow surface temperature can be measured with infrared radiometers and the effective temperature at 6 GHz can be estimated using the 6 GHz brightness temperature. Because of the large temperature gradient in the snow the snow surface temperature is relatively poorly correlated with both the snow-ice interface temperature and the effective temperatures between 6 and 89GHz. However, the effective temperatures between 6 GHz and 89 GHz are highly correlated. The 6 GHz brightness temperature can be related to the snow/ice interface temperature correcting for the temperature dependent penetration depth in saline ice. This snow-ice interface temperature estimate may be more easily used in physical modelling than the effective temperature. The 6 GHz brightness or effective temperature estimates or the snow-ice interface temperature is a closer proxy for the effective temperature near 50 GHz than the snow surface temperature (Tonboe et al. 2011). Based on the simulations in Tonboe et al. (2011) the effective temperature at 50GHz, Teff50v, is:

$$Teff50v = \frac{T6v - 57.06}{0.77} \qquad (21),$$

where T6v is the surface brightness temperature at 6 GHz.

This simulated temperature estimate (Teff50v) which correlates well with the snow ice interface temperature (Tsi) is quite close to the relationship derived by Grönfeldt (2015) from buoy and satellite measurements:

Tsi = 1.23Tv6 – 57.81 (22).

Grönfeldt (2015) also shows that by including the brightness temperature at 10 GHz the standard error between estimate and measurements is reduced compared to single channel relationships. We have therefore derived the following relationship between snow ice interface temperature, Tsi, and 10 and 6 GHz satellite brightness temperature measurements:

Tsi = 1.34Tv6 + 0.05Tv10 – 91.49 (23).

Eq. 23 is used as the effective temperature for generating the validation product and it is provided together with the emissivity product for consistency.

The temperature correlation matrix based on simulations is shown in Table 2 (Tonboe et al., 2011).

	Tair	*Tsnow*	*Tice*	*Teff6v*	*Teff10v*	*Teff18v*	*Teff23v*	*Teff36v*	*Teff50v*	*Teff89v*
Tair	1	0.97	0.78	0.75	0.76	0-77	0.78	0.80	0.84	0.91
Tsnow	0.97	1	0.81	0.78	0.79	0.80	0.81	0.84	0.88	0.95
Tice	0.78	0.81	1	0.99	0.99	0.99	0.99	0.99	0.98	0.95
Teff6v	0.75	0.78	0.99	1	0.99	0.99	0.99	0.99	0.98	0.92
Teff10v	0.76	0.79	0.99	9.99	1	0.99	0.99	0.99	0.98	0.92
Teff18v	0.77	0.80	0.99	0.99	9.99	1	0.99	0.99	0.98	0.93
Teff23v	0.78	0.81	0.99	0.99	0.99	0.99	1	0.99	0.99	0.93
Teff36v	0.80	0.84	0.99	0.99	0.99	0.99	0.99	1	0.99	0.95
Teff50v	0.84	0.88	0.98	0.98	0.98	0.98	0.99	0.99	1	0.97
Teff89v	0.91	0.95	0.95	0.92	0.92	0.93	0.93	0.95	0.97	1

Table 2. The *Teffv* correlation matrix. The 2m air (*Tair*), the physical snow surface (*Tsnow*) and the snow-ice interface (*Tice*) temperatures are included.

12. Processing

The input to the emissivity algorithm are the 18 and 36 GHz brightness temperatures from conically scanning radiometers such as SSM/I SSMIS and AMSR and the output is the R and S parameters defined in equations 17 and 18 respectively. These parameters together with a given incidence angle and polarisation can be used in equations 15 and 16 to compute the sea ice surface emissivity for atmospheric sounders such as SSMIS and AMSU-A.

Input: Tb18v, Tb36v, Tb36h

Summary of the 10 processing steps:

1. The NetCDF format swath data are read.
2. The 37 GHz channels are re-sampled to 19 GHz resolution using a Gaussian weighting function and a circular 'field of view' of 56.5 km.
3. Realistic brightness temperatures for sea ice are selected for further processing:

   160.0 K < Tb19v < 273.15 K

   130.0 K < Tb37v < 273.15 K

   100.0 K < Tb37h < 273.15 K

   (Tb37v - Tb19v) / (Tb37v + Tb19v) < 0.05

   (Tb37v - Tb37h) / (Tb37v + Tb37h) < 0.15
4. Each of the two hemispheres is selected using each of the data point latitudes.
5. The R, S, ev and nadir e are estimated using the model.
6. Data-points where the model yields false emissivities at any angle exceeding 1 or below 0 are excluded and flagged.
7. Each of the new data fields (R, S, ev, nadir e and flags) are appended to the swath file as super-files and written in NetCDF format.
8. The parameters in the swath file are gridded using a nearest neighbour re-sampler.
9. The data are plotted as png-quick looks.
10. The gridded data including Tsi are written as NetCDF format files.

13. Validation/comparison plan

The microwave sea ice emissivity is not measured by any space borne, airborne or in situ devices. Anyway, it affects the thermal microwave emission from the sea ice surface and the top-of-the atmosphere microwave brightness temperature measured by satellites. The near 50.3 GHz and 52.8 GHz channels on a number of atmospheric sounders for example the SSMIS, which is used here, are on the shoulder of the atmospheric oxygen absorption line complex and while the surface emissivity is the same at the two channels they are affected very differently by the intervening atmosphere.

A simplified radiative transfer equation describes the atmospheric and surface emission interaction, so that the brightness temperature, Tb, measured by satellite is:

$$Tb = TBU+\tau(e*Teff + (1-e)TBD) \quad (24),$$

where TBU is the up-welling brightness temperature from the atmosphere, τ is the atmospheric transmissivity, Teff is the surface effective temperature, e is the surface emissivity, and TBD is the down welling atmospheric brightness temperature. Here we wish to estimate e using the Tv50 and the Tv52 SSMIS data, NWP data on temperature and water vapour, and AMSR Tv6 and Tv10 data for comparison with the OSI SAF near 50 GHz sea ice emissivity product.

In essence, the e is estimated iteratively by minimizing the difference between Tb's measured by SSMIS and simulated Tb's at 50.3 GHz vertical polarisation and the 52.8 GHz vertical polarisation using equation 24 and given the water vapour and temperature of the atmosphere from the ECMWF numerical weather prediction model (current near real time operational model) and the AMSR Tv6 and Tv10. SSMIS is a conical scanning radiometer measuring at a constant incidence angle of 53.1 degrees. This continuous validation procedure is in many ways similar to the initial and much shorter period validation of the emissivity product which is described in the validation report and in Tonboe et al. (2013). However, this continuous validation procedure is much more computationally efficient which allows real time validation globally on every ice covered pixel. The three step procedure is:

1. Input data are: SSMIS Tv50 and Tv52, ECMWF total water vapour, and surface air temperature and AMSR2 Tv6 and Tv10.

2. All of the variables in equation 24 except the e are computed based on the input data and a regression RTM.

3. The emissivity, e, is found iteratively using the local adjoint of equation 24. The scheme is solved using two different first guess emissivities (same first guess at the beginning of all iterations) and the physical and radiance covariance for constraints.

The effective surface temperature (Teff in eq. 24) is computed as a linear combination between the brightness temperature at 10GHz (Tv10) and the brightness temperature at 6 GHz (Tv6) in equation 23.

14. Acknowledgements

We would like to thank the two EUMETSAT reviewers Dominique Faucher and Anne O'Caroll and the two external reviewers Fatima Karbou from Meteo France and Chawn Harlow from the UK Met. Office for their constructive comments to this report. ECMWF ERA-40 data used in this study have been obtained from the ECMWF data server. The model was developed within the EU FP 7 Damocles project

and its implementation, testing and validation was done within the EUMETSAT CDOP-1 OSI SAF project. We would also like to thank Leif Toudal Pedersen for reviewing the updated version of this document.

15. References

Aires, F., C. Prigent, F. Bernardo, C. Jimenez, R. Saunders, P. Brunel. 2010. A tool to estimate land surface emissivities at microwaves frequencies (TELSEM) for use in numerical weather prediction. Q. J. R. Meteorol. Soc.

Baunach, T., C. Fierz, P. K. Satyawali, and M. Schneebeli, 2001. A model for kinetic grain growth, Annals of Glaciology 32, 1-6.

Brun, E., E. Martin, V. Simon, C. Gendre, and C. Coleou, 1989. An energy and mass model of snow cover suitable for operational avalanche forecasting. Journal of Glaciology 35(121), 333-342.

Comiso, J. C, D. J. Cavalieri, C. L. Parkinson, and P. Gloersen. 1997. Passive microwave algorithms for sea ice concentration: a comparison of two techniques. Remote Sensing of Environment 60, 357-384.

Drusch, M., T. Holmes, P. de Rosnay, G. Balsamo. 2009. Comparing ERA-40 based L-band brightness temperatures with skylab observations: a calibration/validation study using the community microwave emission model. Journal of hydrometeorology 10, DOI: 10.1175/2008JHM964.1, 213-226.

English, S. J. 1999. Estimation of temperature and humidity profile information from microwave radiances over different surface types. Journal of Applied Meteorology 38, 1526-1527.

English, S. J., The Importance of Accurate Skin Temperature in Assimilating Radiances From Satellite Sounding Instruments, IEEE Trans. Geosci. Remote Sens., vol. 46, no. 2, pp. 403 – 408, Feb. 2008.

Guedj, S., F. Karbou, F. Rabier, A. Bouchard, 2010, Microwave land emissivity over Antarctica : Impact of the surface approximation, IEEE Trans. on Geoscience and Remote sensing, Vol. 48, Issue 4, 1976-1985, 10.1109/TGRS.2009.2036254

Grönfeldt, I. Snow and sea ice temperature profiles from satellite data and ice mass balance buoys. Student thesis series INES nr. 370. p. 70. Lund University, Sweden.

Heygster, G., C. Melsheimer, N. Mathew, L. Toudal, R. Saldo, S. Andersen, R. Tonboe, H. Schyberg, F. Thomas Tveter, V. Thyness, N. Gustafsson, T. Landelius, and P. Dahlgren. 2009. POLAR PROGRAM: Integrated Observation and Modeling of the arctic Sea Ice and Atmosphere. Bulletin of the American Meteorological Society 90, 293 – 297.

Jordan, R., 1991. A one-dimensional temperature model for a snow cover. CRREL SP 91-16.

Karbou, F., E. Gérard, and F. Rabier, 2006, Microwave Land Emissivity and Skin Temperature for AMSU-A & -B Assimilation Over Land, Q. J. R. Meteorol. Soc., vol. 132, No. 620, Part A, pp. 2333-2355(23).

Kunkee, D. B., G. A. Poe, D. J. Boucher, S. D. Swadley, Y. Hong, J. E. Wessel, and E. A. Uliana, 2008. Design and evaluation of the first special sensor microwave imager/sounder, IEEE Transactions on Geoscience and Remote Sensing 46(4), 863-883.

Marbouty, D., 1980. An experimental study of temperature gradient metamorphosism. Journal of Glaciology 26(94), 303-312.

Mathew, N.; Heygster, G.; Melsheimer, C.; Kaleschke, L., 2008: Surface Emissivity of Arctic Sea Ice at AMSU Window Frequencies. IEEE Transactions on Geoscience and Remote Sensing, Volume 46, Issue 8 (Aug. 2008) pp 2298 – 2306.

Mätzler, C. 2005. On the determination of surface emissivity from satellite observations. IEEE Geoscience and Remote Sensing Letters 2(2), 160-163.

Mätzler, C., 1998. Improved Born approximation for scattering of radiation in a granular medium. Journal of Applied Physics 83(11), 6111-6117.

Mätzler, C., 2002. Relation between grain-size and correlation length of snow. Journal of Glaciology 48(162), 461-466.

Mätzler, C., and A. Wiesmann, 1999. Extension of the Microwave Emission Model of Layered Snowpacks to coarse-grained snow, Remote Sensing of Environment 70, 317-325.

Mätzler, C., P. W. Rosenkrantz. 2007. Dependence of Microwave brightness temperature on bistatic surface scattering: model functions and applications to AMSU-A. IEEE Transactions on Geoscience and Remote Sensing 45(7), 2130-2138.

Mätzler, C., P.W. Rosenkranz, A. Battaglia, and J.P. Wigneron, Eds., 2006. Thermal Microwave Radiation - Applications for Remote Sensing, IEE Electromagnetic Waves Series, London, UK.

Maykut, G. A., 1986. The surface heat and mass balance. In: N. Untersteiner (Ed.): The geophysics of sea ice. (pp. 395-464). NATO ASI Series, plenum Press, New York and London.

Maykut, G. A., and Untersteiner, N, 1971., Some results from a time-dependent thermodynamic model of sea ice. J. Geophys. Res., 76, 1550-1575.

Nakawo, M., and N. K. Sinha, 1981. Growth rate and salinity profile of first-year sea ice in the high Arctic. Journal of Glaciology 27(96), 315-330.

Narvekar, P. S., G. Heygster, R. Tonboe, T. J. Jackson. 2011. Analysis of WindSat third and fourth Stokes components over Arctic sea ice. IEEE Transactions on Geoscience and Remote Sensing 49(5), 1627-1636.

Schyberg, H and Tveter, F.T., 2009: Report on microwave ice surface emission modelling using NWP model data. DAMOCLES deliverable report D1.2-02.f, April, 2009. Available from the authors at Norwegian Meteorological Institute, P.O. Box 43-Blindern, NO-0313 Oslo, Norway.

Schyberg, H and Tveter, F.T., 2010: Improved assimilation method in NWP and impact on forecast quality in the Arctic. DAMOCLES deliverable report D4.3-09, June, 2010. Available from the authors at Norwegian Meteorological Institute, P.O. Box 43-Blindern, NO-0313 Oslo, Norway.

Tonboe, R. T. 2010. The simulated sea ice thermal microwave emission at window and sounding frequencies. Tellus 62A, 333-344.

Tonboe, R. T. G. Dybkjær, J. L. Høyer. 2011. Simulations of the snow covered sea ice surface and microwave effective temperature. Tellus 63A, 1028-1037.

Tonboe, R. T., 2005. A mass and thermodynamic model for sea ice. Danish Meteorological Institute Scientific Report 05-10.

Tonboe, R. T., H. Schyberg, E. Nielsen, K. R. Larsen, F. T. Tveter. The EUMETSAT OSI SAF near 50 GHz sea ice emissivity model. Tellus A, 2013, 65, 18380, http://dx.doi.org/10.3402/tellusa.v65i0.18380.

Ulaby, F. T., R. K. Moore, A. K. Fung. 1982. Microwave remote sensing, active and passive, vol. II, Artech House, Norwood MA.

Warren, S. G., I. G. Rigor, N. Untersteiner, V. F. Radionov, N. N. Bryazgin, Y. I. Aleksandrov, and R. Colony, 1999. Snow depth on Arctic sea ice. Journal of Climate 12, 1814-1829.

Weng, F., B. Yan, N. C. Grody. 2001. A microwave land emissivity model. Journal of Geophysical Research 106(D17), 20115-20123.

Wiesmann, A., and C. Mätzler, 1999. Microwave emission model of layered snowpacks, Remote Sensing of Environment 70, 307-316.

Wiesmann, A., C. Fierz, and C. Mätzler, 2000. Simulation of microwave emission from physically modelled snowpacks. Annals of Glaciology 31, 397-404.

Wiesmann, A., C. Mätzler, and T. Weise, 1998. Radiometric and structural measurements of snow samples. Radio Science 33(2), 273-289.